



UNIVERSITY OF LEEDS

This is a repository copy of *Real-Time Hyperbola Recognition and Fitting in GPR Data*.

White Rose Research Online URL for this paper:

<https://eprints.whiterose.ac.uk/102528/>

Version: Accepted Version

Article:

Dou, Q, Wei, L, Magee, D orcid.org/0000-0003-2170-3103 et al. (1 more author) (2017) Real-Time Hyperbola Recognition and Fitting in GPR Data. *IEEE Transactions on Geoscience and Remote Sensing*, 55 (1). pp. 51-62. ISSN 0196-2892

<https://doi.org/10.1109/TGRS.2016.2592679>

(c) 2016 IEEE. Personal use of this material is permitted. Permission from IEEE must be obtained for all other users, including reprinting/ republishing this material for advertising or promotional purposes, creating new collective works for resale or redistribution to servers or lists, or reuse of any copyrighted components of this work in other works

Reuse

Items deposited in White Rose Research Online are protected by copyright, with all rights reserved unless indicated otherwise. They may be downloaded and/or printed for private study, or other acts as permitted by national copyright laws. The publisher or other rights holders may allow further reproduction and re-use of the full text version. This is indicated by the licence information on the White Rose Research Online record for the item.

Takedown

If you consider content in White Rose Research Online to be in breach of UK law, please notify us by emailing eprints@whiterose.ac.uk including the URL of the record and the reason for the withdrawal request.



eprints@whiterose.ac.uk
<https://eprints.whiterose.ac.uk/>

Real Time Hyperbolae Recognition and Fitting in GPR Data

Qingxu Dou, Lijun Wei, Derek R. Magee, and Anthony G. Cohn

Abstract—The problem of automatically recognising and fitting hyperbolae from Ground Penetrating Radar (GPR) images is addressed, and a novel technique computationally suitable for real time on-site application is proposed. After pre-processing of the input GPR images, a novel thresholding method is applied to separate the regions of interest from background. A novel column-connection clustering (C3) algorithm is then applied to separate the regions of interest from each other. Subsequently, a machine learnt model is applied to identify hyperbolic signatures from outputs of the C3 algorithm and a hyperbola is fitted to each such signature with an orthogonal distance hyperbola fitting algorithm. The novel clustering algorithm C3 is a central component of the proposed system, which enables the identification of hyperbolic signatures and hyperbola fitting. Only two features are used in the machine learning algorithm, which is easy to train using a small set of training data. An orthogonal distance hyperbola fitting algorithm for ‘south-opening’ hyperbolae is introduced in this work, which is more robust and accurate than algebraic hyperbola fitting algorithms. The proposed method can successfully recognise and fit hyperbolic signatures with intersections with others, hyperbolic signatures with distortions and incomplete hyperbolic signatures with one leg fully or largely missed. As an additional novel contribution, formulae to compute an initial ‘south-opening’ hyperbola directly from a set of given points are derived, which make the system more efficient. The parameters obtained by fitting hyperbolae to hyperbolic signatures are very important features, they can be used to estimate the location, size of the related target objects, and the average propagation velocity of the electromagnetic wave in the medium. The effectiveness of the proposed system is tested on both synthetic and real GPR data.

Index Terms—GPR, Column-connection clustering algorithm, hyperbola recognition, orthogonal distance fitting, machine learning, buried asset detection.

I. INTRODUCTION

The authors are with the School of Computing, University of Leeds, Leeds, UK, LS2 9JT. email: Q.Dou@leeds.ac.uk (corresponding author), L.J.Wei@leeds.ac.uk, D.R.Magee@leeds.ac.uk, A.G.Cohn@leeds.ac.uk; t: +44 (0)113 343 5430; f: +44 (0)113 343 5468.

As a non-destructive tool for investigation of shallow subsurface, GPR has been widely used in detection and mapping of subsurface utilities such as pipes and cables [1]. There are typically two pattern shapes in B-scan images of GPR, hyperbolic curves and linear segments [2]. Hyperbolic curves are due to objects with a cross-section size of the order of the radar pulse wavelength; linear segments stem from planar interfaces between layers with different electrical impedance. Because of system noise, the heterogeneity of the medium and mutual wave interactions, GPR images are usually noisy. It is a complex task to automatically extract hyperbolae from GPR data. Considerable research has been devoted in this area and many different strategies have been employed to tackle this topic e.g. [3]–[11]. In addition, if the parameters of a hyperbolic signature can be obtained by fitting a hyperbola to it, the parameters can be used to estimate the location and size of the related target object, and the average propagation velocity of the electromagnetic wave in the medium [12].

In [9], [13]–[15], the generalized Hough transform is used to find the parameters of hyperbolae. It is time consuming to determine the parameters of a hyperbola with generalized Hough transform algorithms because the algorithms need to be performed in a space with at least 4 dimensions. In addition, the accuracy of a generalized Hough transform algorithm depends on the discretization of the parameters. Increasing the discretization of the parameters moderately could lead to the computing time increased dramatically. In [16], the generalized Hough transform method was extended to record the associative sets of position/time data pairs that form a contribution to each bin in the Hough accumulator space, which can then be used with a conventional least-squares algorithm to reveal the object position, depth, and radius or velocity. In [17], the edges in the GPR images are detected first and followed by an edge fitting algorithm. This algorithm is only

suitable for very clean GPR images. Otherwise, it would be very difficult to group the points detected from a certain edge for fitting. In [10], an edge detector is also applied to detect edges from GPR images. Although this method can be applied on complex GPR images, in fact, no fitting is applied directly on the detected edge points so only the apexes of the hyperbolae are detected and other parameters of the related hyperbolae are missed, which are essential for identifying other properties of the utilities such as the size of the utilities [12] and even the materials of the utilities [11].

Another type of approach uses machine learning methods to narrow down the regions including hyperbolae in the first step and then a fitting method is applied to find the hyperbola parameters [9], [18]. In [18], after the regions including hyperbolae are extracted with a neural network, an edge detector is employed to detect edges in the extracted regions and then the parameters of hyperbolae are extracted through a generalized Hough transform. In [9], the Viola-Jones algorithm [19] is employed to extract the regions believed to contain hyperbolae, followed by a generalized Hough transform fitting based on the detected edge points. The disadvantages of extracting hyperbola parameters through a generalized Hough transform and edge fitting are pointed out above. In addition, as pointed out by the authors of [9], the quality of detection results depends strongly on the quality and size of the available data for training. The experimental statistics are very impressive with respect to recall and precision for hyperbolae detection and fitting in [7], but the algorithm is only tested with synthetic data generated with GprMax [20] and the scenarios are relatively simple such as no intersection of the hyperbolic signatures is seen in the displayed GPR images. In [21], the authors suggest a probabilistic hyperbola mixture model based on a classification expectation maximization algorithm to extract multiple hyperbolae from a GPR image in one go. There are at least two issues worthy for further consideration. First, compared with an orthogonal circle or ellipse fitting algorithm, orthogonal hyperbola fitting algorithms are more sensitive to the configuration of the given points. The expectation maximization algorithm starts with a general initial partition of the given points, it is difficult to guarantee the convergence of the hyperbola fitting algorithm. Second, the computation of an orthogonal hyperbola fitting algorithm is

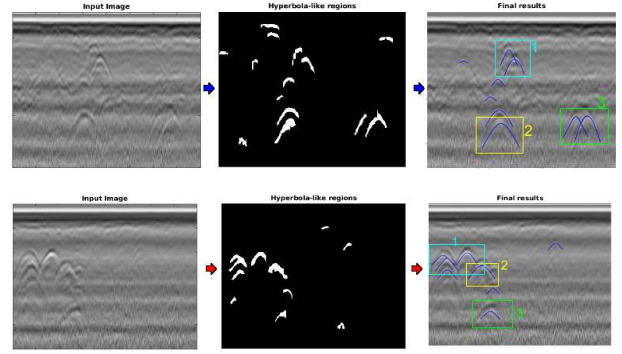


Fig. 1. Examples of difficult scenarios that can be tackled by the proposed hyperbola recognition and fitting method. The first column contains the input GPR images, the second column contains the candidate hyperbolic signatures, and the third column contains the fitted hyperbolae with difficult scenarios, including intersecting hyperbolae in *rectangles 1*, incomplete or distorted hyperbolae in *rectangles 2* and *rectangles 3*.

expensive. In each step the expectation maximization algorithm calls the hyperbola fitting algorithm multiple times.

In this work, we propose a method to automatically detect and fit hyperbolae to GPR images. The proposed multi-stage approach can deal with complex GPR images and especially can recognize and fit hyperbolic signatures in some difficult scenarios as shown in Figure 1, such as hyperbolic signatures with intersections with others, hyperbolic signatures with distortions and incomplete hyperbolic signatures with one leg fully or largely missed, possibly due to local velocity changes. The fitted parameters of the hyperbolic signatures can then be used to estimate the location, size of the related target objects and the average propagation velocity of the signals in the medium for future applications.

The proposed system is composed of four stages, an application of the proposed system is shown in Figure 2. First, a pre-processing procedure is applied to the input image and then a threshold value is selected automatically based on the results of an edge detection. With this threshold value, the regions of interest are separated from the background. With the proposed C3 algorithm, the regions of interest are separated into different clusters. As mentioned above, a hyperbola must be fit to a hyperbolic signature to guarantee convergence. Which regions can be regarded as a hyperbolic signature? A machine learnt model is applied to identify the hyperbolic signatures. As pointed out above, it is necessary to fit a hyperbola to each hyperbolic signature to obtain

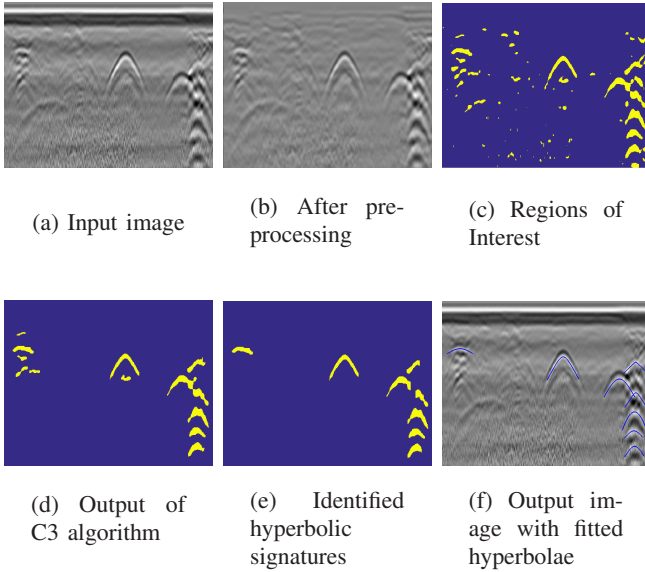


Fig. 2. An illustration of the application of the proposed technique on the bright regions (as described in Section II-A) of a real GPR image. In the first row, (a) the input image, (b) the image after pre-processing, (c) the regions of interest after thresholding. In the second row, (d) clusters after applying C3 algorithm, (e) identified hyperbolic signatures by applying the machine learning algorithm, (f) the output image from the system with fitted hyperbolae Intersecting(with crossing tails, connected without crossing tails), Distorted (asymmetric or incomplete) (best viewed in colour).

the corresponding parameters which can be used to estimate the location and size of the target object, and the signal propagation velocity in the medium [12].

The C3 algorithm is the central component of this work. The previous clustering algorithms are either based on the distance between points [22], [23] or the density of points within a certain area [24], [25]. They are not capable of separating connected regions or segmenting two hyperbola signatures with an intersection. The proposed C3 algorithm is based on matching sequences of elements in adjacent columns with the same row numbers. The output clusters of this algorithm include different combinations of connected blocks and one block can belong to multiple different clusters. With this algorithm, most hyperbolic signatures can be segmented from other regions even if they are connected or have intersections before clustering. Without this step, the proposed machine learning algorithm and hyperbola fitting algorithm can not be applied.

The hyperbola fitting algorithm is also a crucial component of this work. There is a large body of

conic fitting algorithms in the literature [26]–[30]. Compared to algebraic distance, orthogonal distance is invariant to transformations in Euclidean space, therefore orthogonal distance fitting algorithms are more robust and accurate than algebraic distance fitting algorithms [26]. In this work, we introduce a least-squares orthogonal distance fitting algorithm for ‘south-opening’ hyperbolae based on the work of [26]. The efficiency of the fitting algorithm makes this system suitable for real time on-site application. In addition, a novel way to compute the initial hyperbola parameters directly from the given points is introduced. Compared to using algebraic hyperbola fitting results as the initial hyperbola for the orthogonal hyperbola fitting as in [26], [29], [31], the initial hyperbola computed with the proposed method is usually closer to the final fitted one, this makes the fitting algorithm even more efficient.

The rest of this paper is organised as follows. We present the proposed C3 algorithm and the related GPR image pre-processing schemes in section II, which is followed by a description of the machine learning algorithm for hyperbolic signatures identification in section III. The orthogonal distance hyperbola fitting algorithm and the hyperbola initialisation procedure are presented in Section IV. The experimental results are shown and analysed in Section V, and finally, conclusions are drawn in Section VI.

II. A COLUMN-CONNECTION CLUSTERING ALGORITHM

In this section, we present the proposed column-connection clustering (C3) algorithm and the related pre-processing procedures on real data.

A. Adaptive Thresholding of the Input Images

Before applying the proposed clustering algorithm, a series of processing techniques are employed on real GPR images. From Figure 2 (a), it can be seen that some regions including hyperbolic signatures, a strip at the upper part of the image and some small irregular regions have higher responses. It is a common feature for a GPR image to have a bright strip at the top of the image, which is due to the reflectance of the ground surface. In the pre-processing, a moving average filter is applied to the input image to reduce the noise, and then the ensemble mean of each row is subtracted to

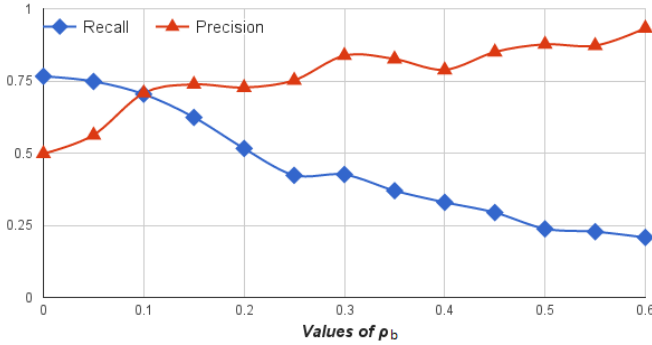


Fig. 3. The illustration of effect of ρ_b in Equation (1) on the values of recall and precision of hyperbola fitting when applying the proposed system on a group of GPR images. Recall = $\frac{tp}{tp+fn}$, precision = $\frac{tp}{tp+fp}$, where tp is the number of correctly fitted hyperbolae by the algorithm, fn is the number of hyperbolae in the ground truth which are not correctly fitted by the proposed algorithm, and fp is the number of fitted hyperbolae not included in the ground truth.

eliminate the bright ground surface reflectance strip. An example image after the pre-processing is shown in Fig. 2 (b). The window size of the filter should not be too large but within a certain range, the experimental results are not that sensitive to it. In our experiments, we tried with 3×3 , 5×5 and 7×7 (in pixels) and very similar results were obtained. The experimental results shown in this paper were done with filter window size of 3×3 .

The regions corresponding to the maxima of positive phase (bright) or minima of negative phase (dark) of the reflected radar signal are the regions of interest for identifying hyperbolae. Since the dark regions of an image corresponding to the bright regions of its inverse image, in the following sections of this paper, we focus on the bright regions representing high responses. If a suitable threshold value can be selected to separate the regions of interest (high responses) from the background, it simplifies further processing. To pick a threshold to separate two regions with different intensities in an image, it is natural to use the intensity value of a pixel on the boundary between these two regions as the threshold. In our work, a large number of regions of interest need to be separated from the background and many boundaries between the regions of interest and the background are involved. We decide to pick a threshold, which relates to the average of the intensity values of the boundary points. First, an edge detector is used to extract the edges between regions of interest and the background to obtain the intensity values of the edge points. If we use the average of all

the edge points as the threshold, then experiments give good recall values but bad precision. If we average by chopping off some darker edge points, the balance between the value of recall and the value of precision improves. But if we chop off too many darker edge points before averaging, the balance worsens. So only the edge pixel intensities which are greater than a certain percentage of the value of the highest edge pixel intensity are used for averaging to obtain the threshold value. The computation of the threshold can be performed with the following expression:

$$threshold_b = mean\{Ie | Ie > \rho_b \times Max_{Ie}\} \quad (1)$$

where $mean$ is a function for computing the average among a set of values, Ie is the intensity value of an edge pixel, Max_{Ie} is the highest edge intensity value and ρ_b is a fraction ($0 < \rho_b < 1$).

The effect of the value ρ_b on the values of recall and precision of fitted hyperbolae when applying the proposed system on a group of real GPR images is demonstrated in Fig. 3. It can be seen that with the value of ρ_b increasing, recall decreases while precision increases. Balancing between these two factors, 0.1 is used in our experiments.

The proposed adaptive thresholding algorithm is also compared with other existing thresholding methods in the literature, which are totally different from each other: the statistical thresholding method in [32], the maximum entropy thresholding method in [33], and the unimodal thresholding method in [34]. The method proposed by Kapur et al in [33] was also used by [11] on GPR images to separate the hyperbola regions from the background. As can be seen in Figure 4(c), it seems that the threshold given by the statistical thresholding method in [32] is too low and it only removes those dark areas; and the threshold given by the maximum entropy thresholding method in [33] is usually too high to retain all the hyperbola regions (Figure 4(b)). The outputs from the unimodal thresholding method [34] (Figure 4(e)) are very similar to those of the proposed method (Figure 4(f)), although based on totally different computation strategies. Further comparison on these two methods with detailed statistics can be found in section V.

With the computed threshold value, the original image is converted into a binary image (e.g. Fig. 2 (c)), which is used for further processing. In a binary image, if the value of a pixel is non-zero,

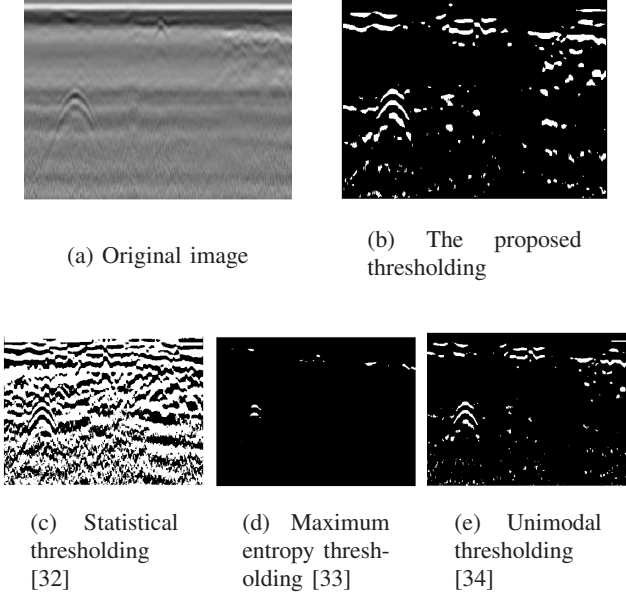


Fig. 4. Comparison of different thresholding methods for bright regions on one real GPR image.

it is regarded as a point. On the other hand, if the value at a pixel is zero, it is regarded as background.

B. Column-connection Clustering (C3) Algorithm

After an input image is converted into a binary one by thresholding, the C3 algorithm is applied to separate the selected regions into different clusters. To explain the C3 algorithm clearly, two concepts should be clarified first: *Column Segment* and *Connecting Elements* of two column segments from adjacent columns.

Column Segment: when searching along a column of a binary image, if the number consecutive points is equal to or higher than a pre-defined number s , then this group is called a column segment. For example, in Figure 5, if the value of s is defined as 4, then there are three column segments along column C_1 . The second group is not a column segment as there are only two consecutive elements in this group. The purpose of selecting a threshold s for column segments is for noise resistance. The criterion to choose it depends on the noise level of the sensor, the radar central frequency and the sampling frequency. Concretely, the maximum value of s is proportional to the sampling frequency f_s and inversely proportional to the radar frequency f_c . An ideal value of s should be bigger than most of the noise but lower than $k \cdot f_s/f_c$ (k is a constant) so

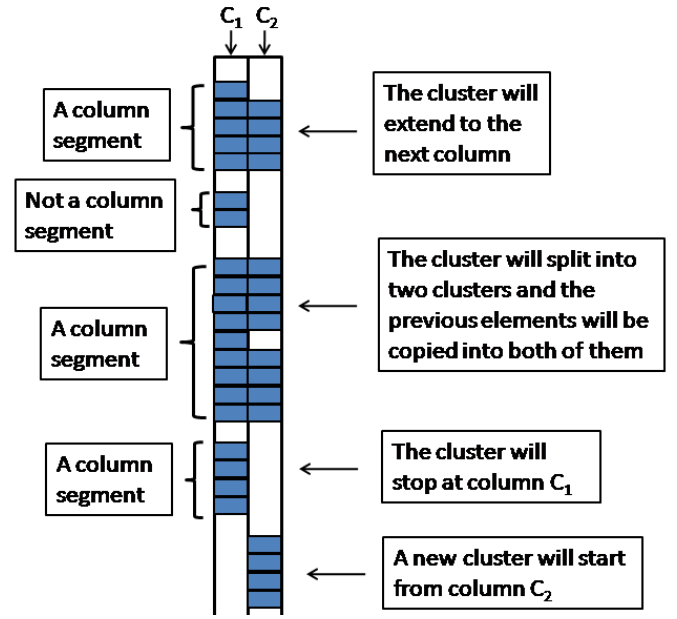


Fig. 5. An illustration of the C3 algorithm (see detailed explanation in the text).

as to reject most of the noise and remain the signal. In our experiments, the value of s is the same for different parts of the image.

Connecting Elements: The location of a point in a certain column segment is defined by its row number. If we say two adjacent column segments have connecting elements, it means they have elements from the same row. In this work we only compare the elements between two column segments which are from adjacent columns. For example, in Figure 5, there are four connecting elements between the first column segments from column C_1 and column C_2 .

In Figure 5, if column C_1 is the first column scanned, then after searching along this column the seeds of three clusters are generated. we call them Cluster 1 to 3 from top to bottom. Next, Column C_2 is scanned and the column segments from this column are obtained. The first column segment from Column C_2 has 4 connecting elements with the first column segment from Column C_1 . If two column segments from adjacent columns have connecting elements, then the cluster extends to the next column to include the elements of the column segment from the later column. Thus, cluster 1 is extended to Column C_2 . There are two column segments of Column C_2 which have 4 connecting elements with Cluster 2 of Column C_1 . In this

situation, Cluster 2 extends to Column C_2 and splits into two clusters Cluster 2_a and Cluster 2_b . All the elements in Cluster 2 are associated with both clusters with the elements in the second column segment of Column C_2 added to Cluster 2_a and the elements in the third column segment of Column C_2 added to Cluster 2_b . As for the third column segment in Column C_1 , since there is no connecting element in Column C_2 with it, Cluster 3 stops at Column C_1 . The fourth column segment in Column C_2 has four elements which is no less than s , and there is no connecting element in the previous Column C_1 , therefore a new cluster starts from Column C_2 with the elements in the fourth column segment as the seeds.

This procedure is performed until the last column is scanned to obtain all the clusters based on column connection. This algorithm is symmetric with respect to the scanning direction, i.e. there is no difference in performing the scanning procedure from left to right or from right to left. The outputs of the clustering algorithm with one GPR image are shown in Figure 6 (b) and (c). For each output cluster from the C3 algorithm, a *central string*, which is the curve connecting the middle points of the elements in each column is computed as shown in Figure 6 (b). The *central string* is a very important feature in C3 algorithm, it is used for further segmentation, machine learning and hyperbola fitting. Physically, the calculated central string corresponds to the peak point of the reflected signal.

The C3 clustering algorithm can separate hyperbolic signatures with intersections. It can be seen in Figure 6, two hyperbolic signatures, which intersect each other, are separated by the C3 algorithm as displayed in Figure 6 (c). This example is based on synthetic data. In real GPR images, the intersections between two hyperbolic signatures are more complicated. In some cases, due to the low strength of response, the parts below the intersection point are missed as the cluster shown within the rectangle window in Figure 7(a). In this situation, the C3 algorithm described so far can not separate them from each other. The whole region is usually identified as a non hyperbolic signature in the machine learning step and two hyperbolae are missed. To deal with this situation, the above mentioned C3 algorithm is extended with a further segmentation step.

Suppose the curve shown in Figure 7(b) is the central string of an output cluster from the first step

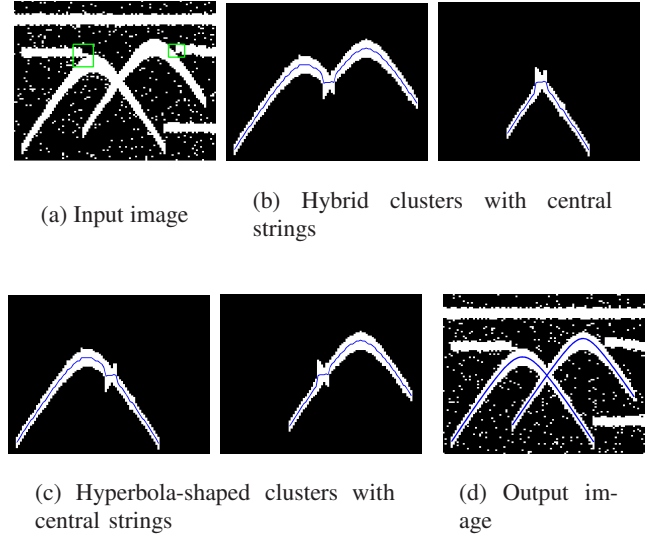


Fig. 6. The application of the proposed system on a synthetic data set. Some output clusters of the C3 algorithm with the central strings are displayed in (b) and (c). The fitted hyperbolae are shown in (d).

of the C3 algorithm. It is similar to the situation where two hyperbolae intersect each other at point P and the parts below point P are not detected. Mathematically, the first derivative at point P is 0 and the second derivative at point P is positive; point P is detected by checking its first and second derivatives and the related cluster is broken at the column corresponding to point P . In the final output of C3 fed to the machine learning algorithm (which will filter out non-hyperbolic shaped responses), the original cluster before this step is also included for avoiding misjudgements.

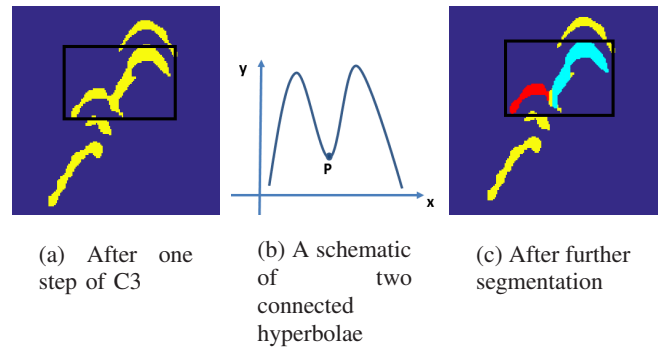


Fig. 7. Further segmentation on connected hyperbola signatures (best viewed in colour).

The C3 algorithm is also helpful for eliminating image noise. From Figure 11, we can see that

the original image is noisy but the images of the separated clusters are clean. This is achieved with the help of pre-defined parameter s . For a reasonable value of s such as 2 or 3, the number of the consecutive noise points along a column is usually not as high as s . Therefore almost all the noisy points are eliminated in the clustering step. By tuning the value of s , the proposed algorithm can deal with images with different noise levels. We tried different values for parameter s in our experiments. The best results were obtained using $s = 3$. So we set s equal to 3 in the shown experimental results.

The pseudo-code of the proposed clustering algorithm can be presented as follows:

```

for i from min_column to max_column do
  if i==min_column
    for j from 1 to num_col_seg_c do
      cell{j,1}=col_seg_c(j);
    end
  else
    for j from 1 to num_col_seg_c do
      record=zeros(1,num_col_seg_p);
      for k=1 to num_col_seg_p do
        n=num_same_elements(col_seg_c(j),
          col_seg_p(k));
        if n>=s && record(j)==0
          cell{j,1}=[cell{j,1} col_seg_c(j)];
          record(j)=1;
        elseif n>=s && record(j)==1
          kk=size(cell,1)+1;
          cell{kk,1}=cell{j};
          cell{kk,1}=[cell{kk,1} col_seg_c(j)];
        elseif n<s
          kk=size(cell,1)+1;
          cell{kk,1}=col_seg_c(j);
        end
      end
    end
  end
end
end
end

```

For a cluster containing one hyperbolic signature, a hyperbola is fitted to this cluster to obtain its parameters. Which output clusters should be regarded as a hyperbolic signature? We answer this question by a machine learnt model for identifying hyperbolic signatures, which is explained in the next section.

III. MACHINE LEARNING ALGORITHM FOR IDENTIFYING HYPERBOLIC SIGNATURES

In this section we present a machine learning method for identifying hyperbolic signatures.

A. Feature Extraction for A Neural Network Classification Algorithm

In order to successfully identify hyperbolic signatures from the outputs of $C3$ algorithm, it is

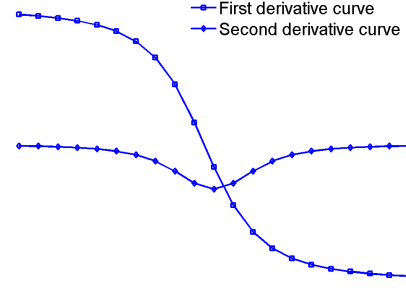


Fig. 8. The first and second derivative curves of a south-opening hyperbola on a domain symmetric to the hyperbola centre. The marker points on each curve make up a template.

necessary to extract attributes that characterise hyperbolic signatures and distinguish them from other undesired clusters and composite clusters of more than one hyperbola.

In a GPR image, the detected hyperbolae are manifested as ‘south-opening’ branches. The general equation of a ‘south-opening’ branch of a hyperbola is written as

$$\frac{(y - y_0)^2}{a^2} - \frac{(x - x_0)^2}{b^2} = 1, \quad \text{with } y < y_0 \quad (2)$$

where y and x relate to the values along the vertical and horizontal axes, the vertical axis y is proportional to the two-way travel time of waves and the horizontal axis x is the distance along the measured direction. (x_0, y_0) is the centre of the hyperbola, a is the length of the semi-major axis and b is the length of semi-minor axis.

The first and second derivatives of the function expressed by equation (2) have the following form:

$$\frac{dy}{dx} = -\frac{a}{b} \frac{x - x_0}{\sqrt{(x - x_0)^2 + b^2}} \quad (3)$$

$$\frac{d^2y}{dx^2} = -\frac{ab}{((x - x_0)^2 + b^2)^{3/2}} \quad (4)$$

The graphs of the functions expressed by equations (3) and (4) on a domain symmetric to the centre of the hyperbola are presented in figure 8. It can be seen that, on a domain symmetric to the centre of a hyperbola, the first derivative and second derivative of a ‘south-opening’ branch of this hyperbola have certain configurations. To determine if a curve is a hyperbola, we can compare the similarity of the first and second derivative configurations of this curve with those of a pre-defined ‘south-opening’ hyperbola with the related

normalized cross correlation (NCC) values. As a typical hyperbola of response from buried utilities, $y^2/25 - x^2/16 = 1$ is used as the pre-defined hyperbola in all the experiments in this work. By testing with different hyperbolae, we found that there is no significant difference if other hyperbolae are used as the pre-defined template hyperbola because NCC is invariant to scaling and the shape of hyperbolae do not change significantly for small sized objects.

When x is discretized in a certain range, the related first and second derivatives of the pre-defined hyperbola make up two vectors, which are used as templates to identify the hyperbolic signatures from the outputs of C3 algorithm. To use the templates, for each output cluster from the C3 algorithm, the central string is computed as shown in Figure 6 (b). NCC values of the first and second derivative values along each central string against the templates are computed after aligning the peaks of the central string and the pre-defined hyperbola curve. The NCC value of two vectors v_1 and v_2 is defined as follows:

$$ncc = \frac{|v_1 \cdot v_2|}{|v_1| * |v_2|} \quad (5)$$

When two ‘south-opening’ hyperbolae are aligned with respect to the x coordinates of their centres, the NCC values of their first and second derivative curves are high (close to 1).

The normalized cross correlation values of the first and second derivatives are used in the following neural network classification step to identify the hyperbolic signatures.

B. Neural Network Classification

A group of positive and negative samples are selected manually from the outputs of C3 algorithm and the two NCC values of each sample are computed, which are used to train a neural network classifier. This stage provides the subsequent stages with a continuous measure of confidence as to whether a particular output of the C3 is a hyperbolic signature or not. First, a three-layer feed-forward perceptron neural network (as in Figure 9) was trained with the backpropagation learning algorithm [35] and the corresponding vectors were recorded. The trained neural network can be applied to classify the outputs of C3 algorithms new to the neural network.

In practice, a smoothed version of the central string is used when comparing with the templates.

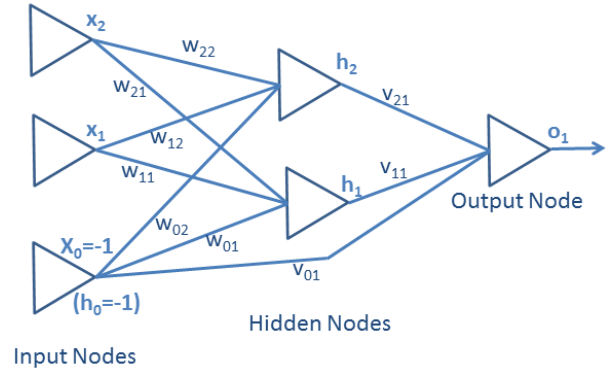


Fig. 9. Neural network diagram.

Judged by the experimental results below in section V, the proposed neural network classification algorithm works very well for most hyperbolic signatures.

IV. ORTHOGONAL DISTANCE HYPERBOLA FITTING

In this section, we present a robust orthogonal distance fitting algorithm for hyperbola fitting [26] and introduce a method to initialize a hyperbola directly from given points.

A. The Hyperbola Fitting Algorithm

Given a set of points $(x_i, y_i)_{i=1}^m$, the orthogonal distance d_i of a point $P_i = (x_i, y_i)$ to a hyperbola can be expressed by

$$d_i^2 = \min_{\phi_i} [(x_i - x(\phi_i))^2 + (y_i - y(\phi_i))^2] \quad (6)$$

where $(x(\phi_i), y(\phi_i))$ is the corresponding closest point of P_i on the hyperbola.

The task is to determine a , b , x_0 and y_0 for this hyperbola by solving

$$\operatorname{argmin}_{a,b,x_0,y_0} \sum_{i=1}^m d_i^2 \quad (7)$$

It is not a trivial task to find the closest point of P_i on a hyperbola when P_i itself is not on this hyperbola as explained below. Suppose $P(x, y)$ is the closest point of P_i on the hyperbola expressed by Equation (2). Since the connecting line of P and P_i is perpendicular to the tangent line of the hyperbola at P , the coordinates of P satisfy the following equation

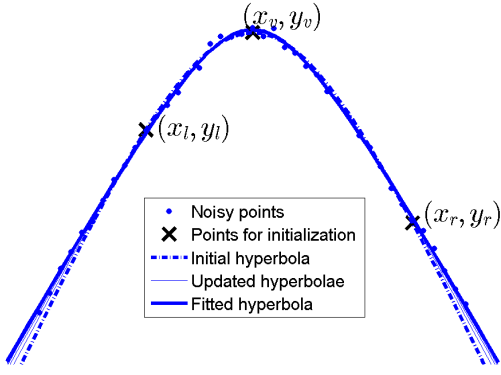


Fig. 10. An example of hyperbola fitting with a synthetic data set.

$$\frac{dy}{dx} \cdot \frac{y_i - y}{x_i - x} = \frac{a^2(x - x_0)}{b^2(y - y_0)} \cdot \frac{y_i - y}{x_i - x} = -1 \quad (8)$$

The coordinates of P can be obtained by solving the system of equations (2) and (8) with a generalized Newton method. The average time needed for finding the closest point of a given point on a hyperbola is about 0.0015 seconds using a computer with Intel 3.6GHz processor coded in Matlab.

After finding the closest point P on the hyperbola for each given point P_i , the coefficients of the hyperbola satisfying Equation (7) can be obtained by using Gauss-Newton iteration

$$\mathbf{J} \cdot \Delta \mathbf{c} = \Delta \mathbf{P} \quad (9)$$

$$\mathbf{c}_{k+1} = \mathbf{c}_k + \lambda \Delta \mathbf{c} \quad (10)$$

where $\mathbf{c} = [a, b, x_0, y_0]^t$ are the parameters of the current hyperbola, $\Delta \mathbf{P} = |\mathbf{P} - \mathbf{P}_i|$ with $\mathbf{P}_i = [x_i, y_i]^t$, a given point, and $\mathbf{P} = [x, y]^t$, the closest corresponding point of \mathbf{P}_i on the current hyperbola. $\mathbf{J} = \frac{\partial F}{\partial \mathbf{c}}|_{\mathbf{c}_k}$ is the Jacobian matrix with F as the corresponding expression of the current hyperbola and λ is the step size parameter.

B. Direct Hyperbola Initialization

In previous work on orthogonal distance fitting, some authors suggest to take the initial parameter values from the corresponding algebraic distance fitting [26], [29]. In this work, because of the robustness of the fitting algorithm and the fact that we only deal with the south-opening branch of a hyperbola from GPR data, we propose a simple and fully automatic procedure to directly compute the parameters of the initial hyperbola which works

very well for converging to the global minimum of Equation 7 in our experiments.

To determine a south-opening branch of a hyperbola, if its apex is given, only two other points, which satisfy certain constraints, are needed.

Given (x_v, y_v) as the coordinates of the apex of a south-opening branch of a hyperbola and (x_l, y_l) as a point on the left hand side of line $x = x_v$ and (x_r, y_r) as a point on the right hand side of the line $x = x_v$, what constraints must be satisfied to determine a hyperbola? Obviously, the following two constraints should be satisfied first: $y_v > y_l$ and $y_v > y_r$. Second, (x_l, y_l) and (x_r, y_r) can not be symmetric to the line of $x = x_v$. The reason will be given later in this section. Third, when x_v, y_v, x_l, y_l and x_r are fixed values, the value of y_r must satisfy Equations (11) and (12).

$$y_r < y_v + \frac{(x_v - x_r) \cdot (y_v - y_l)}{x_v - x_l} \quad (11)$$

$$y_r > \frac{s_l \cdot y_v - s_r \cdot (y_v - y_l)}{s_l} \quad (12)$$

where $s_r = (x_r - x_v)^2$ and $s_l = (x_l - x_v)^2$.

For a given set of points $(x_i, y_i)_{i=1}^m$ for fitting a south-opening hyperbola, to initialize a hyperbola, we first compute three points from the given points. First, the point with largest y-coordinate is found and a centroid is computed among the given points within a neighbourhood of this point. This centroid is used as the apex of the initial hyperbola. Denote its coordinates as (x_v, y_v) , then $x_0 = x_v$ with x_0 the x-coordinate of the centre of the initial hyperbola. Next, pick a region to the left of (x_v, y_v) which includes some given points. Denote the coordinates of the centroid of the given points within this region as (x_l, y_l) , which are also used to compute the initial hyperbola. The same procedure is applied to the right side of (x_v, y_v) to obtain a point (x_r, y_r) . To avoid (x_l, y_l) and (x_r, y_r) being symmetric to line $x = x_v$, the regions picked on both sides of (x_v, y_v) should have different distances to line $x = x_v$. If the value of y_r satisfies Equations (11) and (12), its value is used to initialize the hyperbola, otherwise its value is replaced by the average of the right-hand sides of Equations (11) and (12). Then the other three parameters in Equation (2) can be computed as follows

$$y_0 = \frac{s_l \cdot y_r^2 - s_r \cdot y_l^2 + (s_r - s_l) \cdot y_v^2}{2(y_r \cdot s_l - y_l \cdot s_r + y_v \cdot (s_r - s_l))} \quad (13)$$

$$a^2 = (y_0 - y_v)^2 \quad (14)$$

$$b^2 = \frac{s_r \cdot a^2}{(y_r - y_0)^2 - a^2} \quad (15)$$

where s_r and s_l are the same as in Equation (11) and (12) and y_0 is the y-coordinate of the centre of the initial hyperbola.

If (x_l, y_l) and (x_r, y_r) are symmetric to line $x = x_v$, and then $s_r = s_l$ and $y_r = y_l$. In this situation, the denominator of the right side of Equation (13) is zero. So points (x_l, y_l) and (x_r, y_r) should not be symmetric to line $x = x_v$.

An example of orthogonal distance hyperbola fitting is presented in Figure 10 where the initial hyperbola is computed with the proposed method. Although only three points are used to compute the initial hyperbola, it is reasonably close to the given points. After sufficient steps, the fitting procedure converges. In our experiments, most fittings converge within 100 iterations.

V. EXPERIMENTS

In this section, experimental results on synthetic and real data are displayed and analysed. The computational cost is also analysed in this section.

A. Synthetic Data

First, we applied the proposed algorithm on synthetic data sets. The synthetic data sets are generated to simulate the different scenarios of hyperbolae configuration in GPR images, such as hyperbolae with different shapes and sizes, intersecting hyperbolae with crossing legs, noisy strips and points, etc. In the first experiment (Figure 11), there are two hyperbola-shaped regions and three linear segment regions (Figure 11 (a)). There is no intersection between the two hyperbolic signatures but one of the linear segments is connected to one of the hyperbolic signatures. There are 5 clusters in total given by the C3 algorithm and 4 of them are displayed in Figure 11 (b) and (c). From the output clusters, it can be seen that the hyperbolic signature, which is connected to a linear segment region, is separated from it (Figure 11 (c)).

In the second experiment (see Figure 6), besides the connections of a hyperbolic signature with the linear segment regions, there is an intersection between the hyperbolic signatures in the input image.

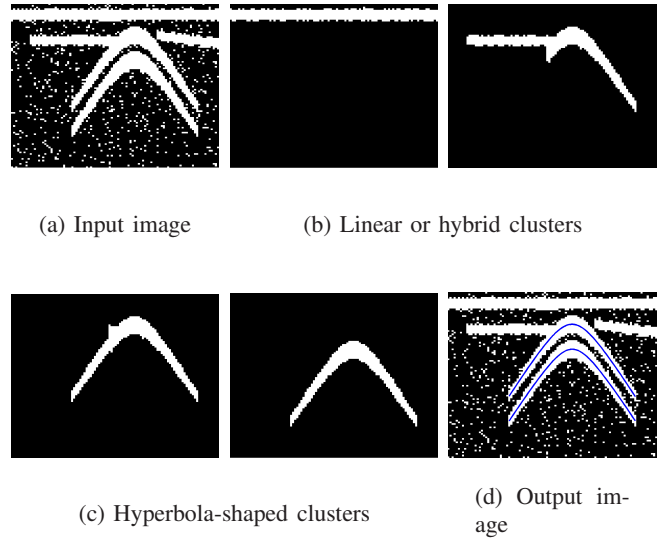


Fig. 11. The illustration of the application of the proposed system on a synthetic data set.

TABLE I
EXPERIMENTAL RESULTS ON SYNTHETIC DATA.

| Ground truth | True positive | False positive |
|--------------|---------------|----------------|
| 52 | 52 | 3 |

The experimental result demonstrates that the hyperbolic signatures can be clearly separated from each other by the C3 algorithm (Figure 6 (c)). In Figure 6 (b) and (c), the central string of the corresponding clusters are also displayed. In our experiments, a smoothed version of each central string is used in the neural network classification algorithm for identifying hyperbolic signatures.

More experimental results on synthetic data sets are displayed in Figure 12. It can be seen that all the hyperbolic signatures are detected. In the synthetic data, there are many intersections between different hyperbola branches. For each such intersection, a cluster is obtained through the C3 algorithm such as the one displayed in the right image in Figure 6 (b). Most of them are classified correctly by the neural network classification algorithm as non hyperbolic signatures and only few of them are regarded as hyperbolic signatures such as the red curve in the first image in Figure 12. Precise statistics are given in Table I. For the correctly classified hyperbolic signatures, the proposed hyperbola fitting algorithm converges to the global minimum in all cases.

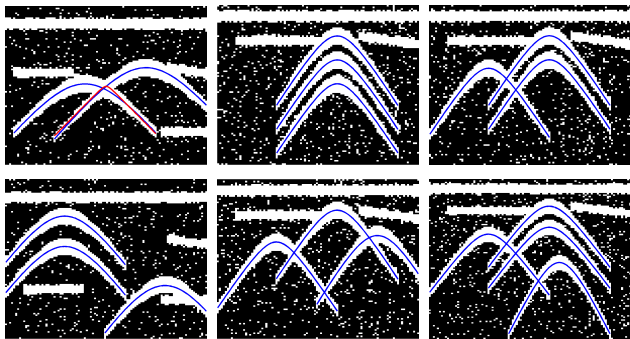


Fig. 12. Some experimental results on synthetic data (Best viewed in colour).

B. Real Data

We also applied our algorithms to real data sets. For a real data set, a thresholding step needs to be applied to separate the regions of high response from the background (Figure 4). After this step, the remaining procedures are the same as those of the synthetic data.

In the real dataset, 100 GPR images were collected from an externally provided data set. The images contain hyperbolae at different depths, some of them are clear and well-shaped, some are weakly contrasted and asymmetric with numerous interactions between each other. 464 hyperbolae were manually annotated from these images. They are used as the ground truth for training and testing. With this group of real data set, 10 fold cross evaluation were performed. More details of the experimental results are given in the following sections.

To facilitate the evaluation of the experimental results with the ground truth, we use a simple way to represent hyperbolae in the ground truth. For each hyperbola in the ground truth, three points are marked manually: the apex, one point on the left hand side of the apex, and another point on the right hand side of it (Figure 13). All the coordinates of the marked points are recorded in a text file with respect to different images. For a fitted hyperbola in a certain test image, if a group of three marked points for ground truth are found with average distance to that hyperbola less than 10 pixels, this hyperbola is regarded as a true positive otherwise it is taken as a false one.

Some experiments on real datasets with the proposed method are displayed in Figures 2, 14, and 16. There are 57 clusters given by the C3 algorithm in the experiment displayed in Figure 2 and 45

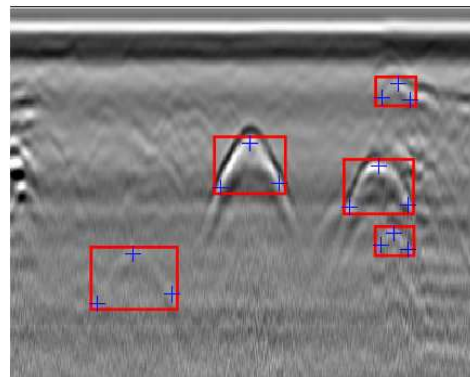


Fig. 13. Example of ground truth in GPR images (Best viewed in colour).

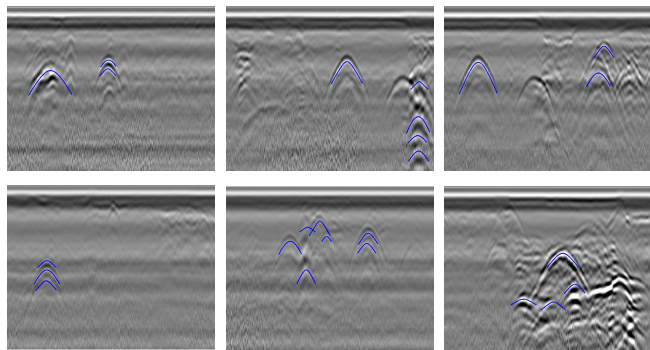
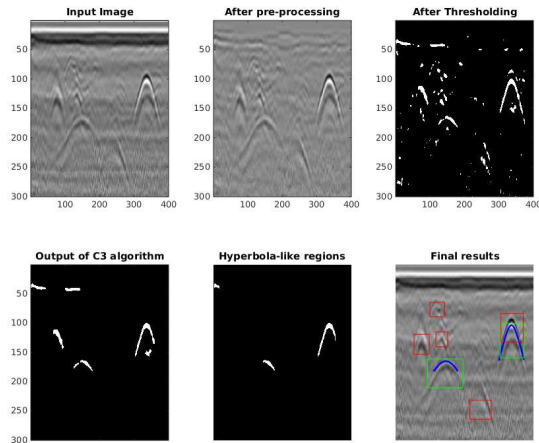
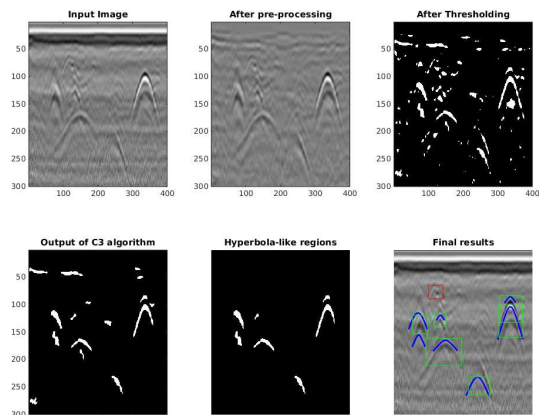


Fig. 14. Some experimental results on real data (Best viewed in colour).

clusters in the experiment displayed in Figure 16. Compared with the synthetic data, the real data are much more noisy. So there are more output clusters in the real data experiments. The pre-processing step captured regions including most of the expected hyperbolae, and the neural network classification algorithm works effectively to pick most of the expected hyperbolic signatures for hyperbola fitting. For a comparison, experiments are repeated by replacing the proposed thresholding method with the unimodal thresholding method introduced in [34]. It can be seen in Figure 15, the thresholding method proposed in this paper can keep more hyperbola regions than the unimodal thresholding. Detailed statistics are given in Table II. It can be seen that among the 10 random trials, the average detection rate and precision rate of the proposed method are higher than those of the unimodal thresholding method.



(a) Results with the unimodal thresholding

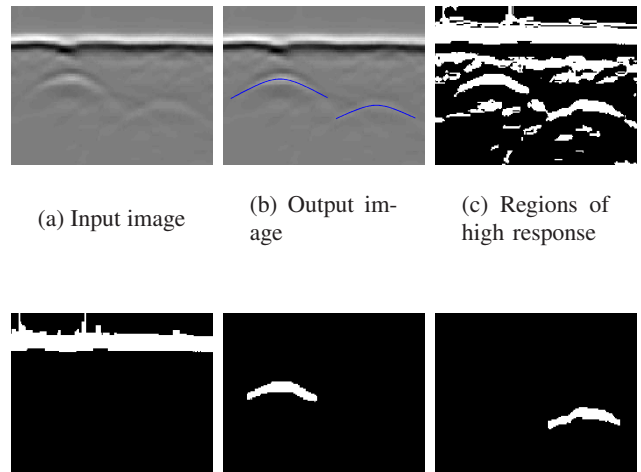


(b) Results with the proposed thresholding

Fig. 15. Comparison of different thresholding methods on one real GPR image: blue curves are the fitted hyperbolae, green rectangles are the correctly found hyperbolae, red rectangles are the hyperbolae missed by the detection algorithm (Best viewed in colour).

C. Comparison of Hyperbola Detection and Fitting Rates with Another Method

We also compared the proposed method with the one introduced in [9]. In [9], a Viola-Jones based detector is used to detect the candidate hyperbola regions at first, and then a generalized Hough transform is used to extract hyperbola parameters by fitting hyperbolic edges of each candidate region. As it did not provide any details of the Hough transform based hyperbola fitting results, we compare this method with our proposed method using two metrics: the detection rate and fitting rate. As mentioned above, if a group of three marked hyperbola points for ground truth are found with average distance



(d) Some output clusters of the C3 algorithm

Fig. 16. An illustration of the application of the proposed technique on a real GPR image. (a) the input image, (b) output image and (c) the regions of interest. (d) Some clusters obtained from the C3 algorithm (not all clusters from the C3 algorithm are shown here (Best viewed in colour)).

to a fitted hyperbola less than 10 pixels, the fitted hyperbola is regarded as a true positive otherwise it is taken as a false one. Since in the proposed method, if a cluster is identified as a hyperbolic signature, a hyperbola is always fitted to that region. So the detection rate and fitting rate of the proposed method are the same. But an obvious difference can be found in the detection rate and fitting rate with the methods proposed in [9].

1) *Detection Rate:* When we mark the three points for each hyperbola in the ground truth, a rectangular bounding box with its sides parallel to the axes is generated with the marked points. An enlarged rectangle window with 5 pixels offset from each side of the bounding box is also recorded as shown in Figure 13 for later use. For the method in [9], if a detected region has more than 60% percent overlap with any recorded rectangle window in the ground truth, it is considered as a correct detection. For training purposes, the rectangle windows related to training images are also used to crop the hyperbola regions and saved as positive samples. 3000 negative samples are also randomly generated from the background regions. When using the Haartraining package of OpenCV to train the classifier, a basic resolution of 24×24 pixels of each region is used in the training procedure. Then,

the obtained classifier is used to detect candidate regions in the testing data set. Detailed statistics of the average detection rate of the method used in [9] are given in the first row of Table II. It can be seen that the detection rate is 0.72, but the average precision rate is only 0.35.

TABLE II

COMPARISON OF THE AVERAGE DETECTION RATES AND FITTING RATES AMONG DIFFERENT METHODS

| Method | Recall | Precision | F-Measure |
|----------------------------|--------|-----------|-----------|
| Detection rates of [9] | 0.724 | 0.347 | 0.474 |
| Fitting rates of [9] | 0.418 | 0.091 | 0.149 |
| Fitting rates of [34] + C3 | 0.638 | 0.654 | 0.643 |
| Fitting rate of our method | 0.704 | 0.708 | 0.702 |

2) *A generalized Hough Transform Based Fitting Rate:* As presented in [9], the candidate regions are smoothed with a Gaussian filter to reduce noise and artefacts, and then converted with a Canny edge detector into a binary image. After that, a generalized Hough transform is used to fit hyperbolae based on the edge points. For each candidate region, only the best hyperbola given by the generalized Hough transform is fitted. Each fitted hyperbola is then compared with the ground truth with the same criterion as described above. It can be seen in some cases that even a correct region is detected in the detection step the generalized Hough transform fails to fit the correct hyperbola, as shown in Figure 18. The recall rates of the correctly fitted hyperbola from different methods are shown in the second column of Table II and Figure 17. In Figure 17, the two images on the first row are only used to demonstrate the original GPR image overlapped with the detected candidate regions from Viola-Jones based detector, and the figures on the second row are the enlarged windows of the red rectangles in the images on the first row. The top horizontal pattern of the GPR image has no influence on the generalized Hough transform results since each candidate region was then cropped and processed separately for hyperbola fitting.

D. Computational time

The size of the synthetic input images is 100×100 pixels. The average computational time of the experiments on one sample image using a computer with Intel 3.6GHz processor is approximately 0.43 seconds. The computational time on real images

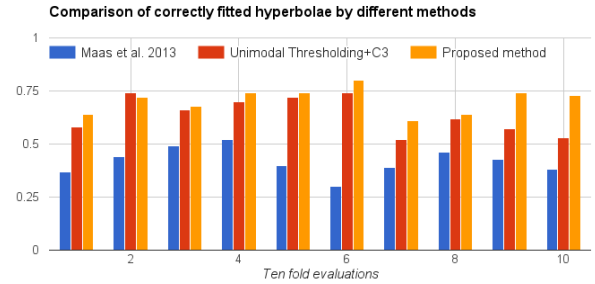


Fig. 17. Comparison of the fitting rates of different methods on 10 cross evaluations.

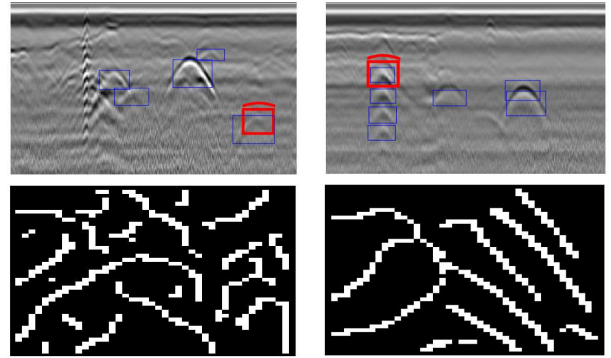


Fig. 18. The generalized Hough transform fails to fit correct hyperbolae in some detected regions. First row: input GPR images with the ground truth marked by blue rectangles. The red curve is the fitted hyperbola to the region in the red window based on the edge points as shown in the second row. It can be seen the fitted hyperbolae are outside the detected region and are regarded as false fitting (Best viewed in colour).

depend on how many hyperbolae are detected. In our experiments, the sizes of the real input images are 300×400 pixels and the computational time of a real image is on average $0.48 + 0.73 \times n$ seconds with n being the number of candidate hyperbolae for fitting; on average 6 hyperbolae were detected and fitted in each test image. This speed is fast enough for real time on-site applications.

As mentioned above, the computation time of the generalized Hough transform based hyperbola fitting method highly depends on the discretization of the parameters. Table III shows the computation time of the generalized Hough transform method when only changing the discretization of the parameters (a, b, x_0, y_0) of Equation (1). In this table $ds = (d_a, d_b, d_{x_0}, d_{y_0})$ denotes the discretization steps of the parameters. It can be seen when $ds = (0.2, 0.2, 0.2, 0.2)$ the average computation time is about 15 minutes, which is not comparable with the proposed method.

TABLE III
COMPUTATION TIME OF HYPERBOLA FITTING USING A
COMPUTER WITH INTEL 3.6GHZ PROCESSOR

| Method | Fitting time per hyperbola (s) | |
|--|--------------------------------|-------------|
| | Discretization values of d_s | Time |
| Generalized Hough transform based fitting method | $ds = (1, 1, 1, 1)$ | 2.97 |
| | $ds = (1, 1, 0.5, 0.5)$ | 11.4 |
| | $ds = (0.5, 0.5, 0.5, 0.5)$ | 47.3 |
| | $ds = (0.2, 0.2, 0.2, 0.2)$ | 895.3 |
| Proposed hyperbola fitting method | | 0.73 |

VI. CONCLUSIONS AND FUTURE WORK

In this paper a novel technique for automatic interpretation of GPR images is introduced. The proposed system¹ allows for the detection of the presence of underground buried objects and can obtain hyperbola parameters by fitting a hyperbola to each hyperbolic signature in a completely automatic manner. The C3 algorithm is based on the connecting elements from adjacent columns of the image which is different from conventional distance/density based clustering techniques. It can not only cluster the separated hyperbolic signatures but also segment intersected or connected hyperbolic signatures into separated ones. The neural network classification algorithm for identifying hyperbolic signatures needs only two features and can be trained easily with a small set of training data. The orthogonal distance hyperbola fitting algorithm is robust and efficient for fitting ‘south-opening’ hyperbolae. The hyperbola parameters obtained through the orthogonal distance fitting algorithm can be used in further applications such as estimating the size of the objects [12]. Despite the intrinsic complexity of GPR images, the experimental results show that the proposed method exhibits very good performance compared with a state of the art method, in terms of robustness to noise, efficiency and accuracy and is fast enough for real time on-site applications. The proposed thresholding method works very well compared with other classic thresholding methods, but we believe a “multi-level thresholding” method which we are currently studying may improve the current method even further by adaptively segmenting the weak reflections such as those from small plastic pipes.

¹The code will be placed in an open source repository.

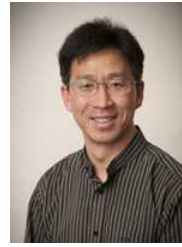
ACKNOWLEDGEMENTS

The financial assistance of the EPSRC under grants EP/F06585X/1 and EP/K021699/1, and the EU under Grant Agreement 280712 is gratefully acknowledged.

REFERENCES

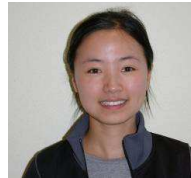
- [1] D. Daniels, *Ground penetrating radar*. London, U. K.: The Inst. Elect. Eng. (IEE), 2004.
- [2] C. Bruschini, B. Gros, F. Guerne, P. Y. Pièce, and O. Carmona, “Ground penetrating radar and imaging metal detector for antipersonnel mine detection,” *Journal of Applied Geophysics*, vol. 40, no. 1-3, pp. 59–71, 1998.
- [3] G. Ciocchetto, S. Delbo, P. Gamba, and D. Roccatto, “Fuzzy shell clustering and pipe detection in ground penetrating radar data,” *IGARSS’99*, vol. 5, pp. 2575–2577, 1999.
- [4] E. Costamagna, P. Gamba, and E. Lossani, “A neural network approach to the interpretation of ground penetrating radar,” *IGARSS’98*, vol. 1, pp. 412–414, 1998.
- [5] P. Gamba and S. Lossani, “Neural detection of pipe signatures in ground penetrating radar images,” *IEEE Transactions on Geoscience and Remote Sensing*, vol. 38, pp. 790–797, 2000.
- [6] R. Janning, T. Horvath, A. Busche, and L. Schmidt-Thieme, “Gamrec a clustering method using geometrical background knowledge for GPR data preprocessing,” *Artificial Intelligence Applications and Innovations (IFIP Advances in Information and Communication Technology 381)*, pp. 347 – 356, 2012.
- [7] R. Janning, A. Busche, T. Horvath, and L. Schmidt-Thieme, “Buried pipe localization using an iterative geometric clustering on GPR data,” *Artificial Intelligence Review*, vol. 42, pp. 403–425, 2013.
- [8] R. Janning, T. Horvath, A. Busche, and L. Schmidt-Thieme, “Pipe localization by apex detection,” *Proceedings of the IET international conference on radar systems*, pp. 1 – 6, 2012.
- [9] C. Maas and J. Schmalzl, “Using pattern recognition to automatically localize reflection hyperbolas in data from ground penetrating radar,” vol. 58, pp. 116–125, 2013.
- [10] L. Mertens, R. Persico, L. Matera, and S. Lambot, “Automated detection of reflection hyperbolas in complex GPR images with no a priori knowledge on the medium,” *IEEE Transactions on Geoscience and Remote Sensing*, vol. 54, no. 1, pp. 580–596, 2016.
- [11] E. Pasolli, F. Melgani, and M. Donelli, “Automatic analysis of GPR Images: a pattern-recognition approach,” *IEEE Transactions on Geoscience and Remote Sensing*, vol. 47, no. 7, pp. 2206–2217, 2009.
- [12] S. Shihab and W. Al-Nuaimy, “Radius estimation for cylindrical objects detected by ground penetrating radar,” *Sensing and Imaging: An International Journal*, vol. 6(2), pp. 151–166, 2005.
- [13] J. Illingworth and J. Kittler, “A survey of the hough transform,” *Computer vision, graphics, and image processing*, vol. 44, no. 1, pp. 87–116, 1988.
- [14] L. Capineri, P. Grande, and J. A. G. Temple, “Advanced image-processing technique for real-time interpretation of ground-penetrating radar images,” *International Journal of Imaging Systems and Technology*, vol. 9, no. 1, pp. 51–59, 1998.
- [15] P. Falorni, L. Capineri, L. Masotti, and G. Penilli, “3-d radar imaging of buried utilities by features estimation of hyperbolic diffraction patterns in radar scans,” *Proceeding of 10th Int. Conf. GPR*, vol. 1, pp. 403–406, 2004.

- [16] C. G. Windsor, L. Capineri, and P. Falorni, "A data pair-labeled generalized Hough transform for radar location of buried objects," *IEEE Geoscience and Remote Sensing Letters*, vol. 11, no. 1, pp. 124–127, Jan 2014.
- [17] M. Fritze, "Detection of buried landmines using ground penetrating radar," *SPIE proceedings*, vol. 2496, pp. 100–108, 1995.
- [18] W. Alnuaimy, Y. Huang, M. Nakhkash, M. Fang, V. Nguyen, and A. Erisken, "Automatic detection of buried utilities and solid objects with GPR using neural networks and pattern recognition," *Journal of Applied Geographics*, vol. 43, pp. 157–165, 2000.
- [19] P. Viola and M. J. Jones, "Robust real-time face detection," *International Journal of Computer Vision*, vol. 57, no. 2, pp. 137–154, 2004.
- [20] A. Giannopoulos, "Modelling ground penetrating radar by gprMax," *Construction and Building Materials*, vol. 19, no. 10, pp. 755–762, 2005.
- [21] H. Chen and A. G. Cohn, "Probabilistic robust hyperbola mixture model for interpreting ground penetrating radar data," in *IEEE World Congress on Computational Intelligence*, 2010, pp. 3367–3374.
- [22] T. Kanungo, D. M. Mount, N. S. Netanyahu, C. D. Piatko, R. Silverman, and A. Y. Wu, "An efficient k-means clustering algorithm: analysis and implementation," *IEEE Trans. Pattern Analysis and Machine Intelligence*, vol. 24, pp. 881–892, 2002.
- [23] R. Ng and J. Han, "Efficient and effective clustering methods for spatial data mining," *Proc. 20th Int. Conf. on Very Large Data Bases*, pp. 144–155, 1994.
- [24] M. Ester, H.-P. Kriegel, J. Sander, and X. Xu, "A density-based algorithm for discovering clusters in large spatial databases with noise," *The Second International Conference on Knowledge Discovery and Data Mining (KDD-96)*, pp. 226–231, 1996.
- [25] L. Ertöz, M. Steinbach, and V. Kumar, "Finding clusters of different sizes, shapes, and densities in noisy, high dimensional data," in *Proceedings of Second SIAM International Conference on Data Mining*, 2003.
- [26] S. Ahn, W. Rauh, and H.-J. Warnecke, "Least-squares orthogonal distance fitting of circle, sphere, ellipse, hyperbola and parabola," *Pattern Recognition*, vol. 34, pp. 2283–2303, 2001.
- [27] F. L. Bookstein, "Fitting conic sections to scattered data," *Computer Graphics and Image Processing*, vol. 9(1), pp. 56–71, 1979.
- [28] A. Fitzgibbon, M. Pilu, and R. B. Fisher, "Direct least square fitting of ellipses," *IEEE Transactions on Pattern Analysis and Machine Intelligence*, vol. 21(5), pp. 476–480, 1999.
- [29] W. Gander, G. Golub, and R. Strebler, "Least-squares fitting of circles and ellipses," *BIT*, vol. 34, pp. 558–578, 1994.
- [30] M. Pilu, A. Fitzgibbon, and R. B. Fisher, "Ellipse-specific direct least-square fitting," in *Proceedings of International Conference on Image Processing*, vol. 3, 1996.
- [31] H. Chen and A. G. Cohn, "Probabilistic conic mixture model and its applications to mining spatial ground penetrating radar data," in *Workshops in SIAM Conference on Data Mining (SDM10)*, 2010.
- [32] N. Otsu, "A Threshold Selection Method from Gray-level Histograms," *IEEE Transactions on Systems, Man and Cybernetics*, vol. 9, no. 1, pp. 62–66, 1979.
- [33] J. Kapur, P. Sahoo, and A. Wong, "A new method for gray-level picture thresholding using the entropy of the histogram," *Computer Vision, Graphics, and Image Processing*, vol. 29, no. 3, pp. 273 – 285, 1985.
- [34] P. L. Rosin, "Unimodal thresholding," *Pattern Recognition*, pp. 2083–2096, 2001.
- [35] J. M. Zurada, *Introduction to Artificial Neural Systems*. USA: West Publishing, 1992.



emathical modelling.

Qingxu Dou Dr Qingxu Dou is currently a research fellow in the School of Computing at University of Leeds, UK. He obtained his MSc in Applied Mathematics from Heriot-Watt University in 2006, a PhD in Electric and Electronic Engineering from Heriot-Watt University in 2011. His research areas of interest are computer vision, sensor data interpretation, data fusion, buried utilities mapping and math-



Lijun Wei Dr Lijun Wei is a research fellow in Computer Science at the University of Leeds, UK. She obtained BSc degree from Wuhan University in China, and a PhD from University of Technology of Belfort and Montbéliard, France. Her main areas of interest are image processing and multi-sensor fusion especially on mapping and intelligent vehicle localization/navigation.



officer of Medical Image Analysis company HeteroGenius Ltd.

Derek R. Magee Dr Derek Magee is a lecturer in Computer Science at the University of Leeds, UK. He obtained a first class BSc Engineering degree from Durham University in 1995, and a PhD from the University of Leeds in 2001. His main areas of interest are image analysis and machine learning in particular applied to Medical Image and Remote sensing data. Additionally, he is chief technical



Sensor Fusion, and Decision Support Systems. Part of his research has focussed on streetworks and utilities for more than a decade. The VAULT system which provides 24/7 real time integrated utility data across Scotland arising from his Mapping the Underworld and VISTA projects won a IET Innovation Award and a NJUG award for "Avoiding Damage". He has received Distinguished Service awards from IJCAI and AAAI.

Anthony G. Cohn Anthony Cohn is a Full Professor in the School of Computing at the University of Leeds and is a Fellow of the Royal Academy of Engineering, the Association for Advancement of Artificial Intelligence, and the European Association for Artificial Intelligence. His research interests are in Artificial Intelligence, Knowledge Representation and Reasoning, Cognitive Vision, Robotics,